

The hydrogen bond network of water supports propagating optical phonon-like modes

Daniel C. Elton^{1,2, a)} and Marivi Fernández-Serra^{1,2, b)}

¹⁾Department of Physics and Astronomy, Stony Brook University, Stony Brook, New York 11794-3800, USA

²⁾Institute for Advanced Computational Sciences, Stony Brook University, Stony Brook, New York 11794-3800, USA

The local structure of liquid water as a function of temperature is a source of intense research. This structure is intimately linked to the dynamics of water molecules, which can be measured using Raman and infrared spectroscopies. The assignment of spectral peaks depends on whether they are collective modes or single molecule motions. Vibrational modes in liquids are usually considered to be associated to the motions of single molecules or small clusters. Using molecular dynamics simulations we find dispersive optical phonon-like modes in the librational and OH stretching bands. We argue that on subpicosecond time scales these modes propagate through water's hydrogen bond network over distances of up to two nanometers. In the long wavelength limit these optical modes exhibit longitudinal-transverse splitting, indicating the presence of coherent long range dipole-dipole interactions, as in ice. Our results indicate the dynamics of liquid water have more similarities to ice than previously thought.

The local structure and dynamics of liquid water as a function of temperature remains a source of intense research and lively debate.¹⁻⁶ A thus far unrecognized discrepancy exists between the peak assignments reported in Raman spectra with those reported in dielectric/IR spectra. Although early experimentalists fit the Raman librational band with two peaks,⁷ it is better fit with three (Supplementary Table 1).⁸⁻¹² Previously these three peaks were assigned to the three librational motions of the water molecule - twisting ($\approx 435 \text{ cm}^{-1}$), rocking ($\approx 600 \text{ cm}^{-1}$) and wagging ($\approx 770 \text{ cm}^{-1}$).^{8,9,11} However, when comparing these assignments to infrared and dielectric spectra, one runs into a serious discrepancy. One expects to find the two higher frequency modes to be present, since only the rocking and wagging librations are IR active. The twisting libration, consisting of a rotation of the hydrogen atoms around the C2 axis, is not IR active since it does not affect the dipole moment of the molecule. Instead, IR spectra show two peaks at 380 and 665 cm^{-1} ,¹³ and similarly dielectric spectra show peaks at 420 and 620 cm^{-1} ,¹⁴ in disagreement with this assignment.

The assignment of longitudinal optical phonon modes to Raman spectra can be made by looking at the longitudinal dielectric susceptibility. This method has been used previously to assign longitudinal phonon modes to the Raman spectra of ice Ih,¹⁵⁻¹⁷ ice Ic,¹⁸ and vitreous GeO₂ and SiO₂.¹⁹ It has previously been shown that the librational peak in the longitudinal dielectric susceptibility of water is dispersive,²⁰ and Bopp & Kornyshev noted that the dispersion relation has the appearance of an optical phonon mode.²¹ The longitudinal mode in the dielectric susceptibility is equivalent to the dispersive mode discovered by Ricci et al. (1989) in the spectrum

of hydrogen density fluctuations.²²

Comparison of peak positions in longitudinal and transverse dielectric susceptibilities often reveals longitudinal-transverse (LO-TO) splitting. LO-TO splitting indicates the presence of long-range dipole-dipole interactions in the system. One way to understand LO-TO splitting is through the Lyddane-Sachs-Teller (LST) relation:²³

$$\frac{\omega_{\text{LO}}^2}{\omega_{\text{TO}}^2} = \frac{\varepsilon(0)}{\varepsilon_\infty} \quad (1)$$

Although this relation was originally derived for a cubic ionic crystal it was later shown to have very general applicability,^{24,25} and has been applied to disordered and glassy solids.^{17,26,27} To apply this equation to water we must use a generalized LST relation which takes into account all of the optically active modes in the system and the effects of dampening.²⁴ The generalized LST relation is:²⁴

$$\prod_i \frac{\omega_{\text{LD}i}}{\omega_{\text{TD}i}} \prod_j \frac{|\bar{\omega}_{\text{L}j}|^2}{\omega_{\text{T}j}^2} = \frac{\varepsilon(0)}{\varepsilon_\infty} \quad (2)$$

Here the index i runs over the Debye peaks in the system and the index j runs over the number of damped harmonic oscillator peaks. The longitudinal frequencies of the damped harmonic oscillators must be considered as complex numbers ($\bar{\omega}_{\text{L}i} = \omega_{\text{L}i} + i\gamma_i$), where γ_i is the dampening factor.

As shown by Barker, the generalized LST equation can be understood purely from a macroscopic point of view,²⁴ so by itself it yields little insight into microscopic dynamics. LO-TO splitting can be understood from a microscopic standpoint via the equation:^{28,29}

$$\omega_{\text{L}k}^2 - \omega_{\text{T}k}^2 = \frac{4\pi C}{3v} \left(\frac{\partial \mu}{\partial Q_k} \right)^2 \quad (3)$$

^{a)}Electronic mail: daniel.elton@stonybrook.edu

^{b)}Electronic mail: maria.fernandez-serra@stonybrook.edu

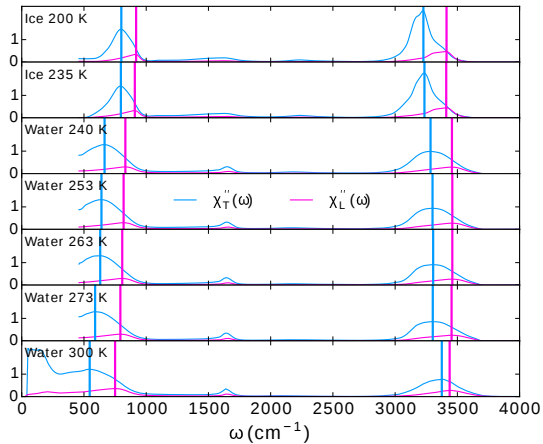


FIG. 1. **Dielectric susceptibilities of ice and water.** Computed from index of refraction data using equations 4 and 6. data from 210 to 280 K comes from aerosol droplets³¹ while the data at 300 comes from bulk liquid.³²

Here v is the volume per unit cell, Q_k is the normal coordinate of mode k , and C is a prefactor which depends on the type of lattice and the boundary conditions of the region being considered (for an infinite cubic lattice, $C = 1$). Equation 3 shows that LO-TO splitting is intimately related to crystal structure, and it has been used to evaluate the quasi-symmetry of room temperature ionic liquids.³⁰

In this work we show how the dielectric susceptibility can be used to probe water’s local structure and dynamics. Our work solves the aforementioned peak assignment discrepancy. We find that the lowest frequency librational Raman peak ($\approx 435 \text{ cm}^{-1}$) is a transverse optical phonon-like mode while the highest frequency peak ($\approx 770 \text{ cm}^{-1}$) is a longitudinal optical phonon-like mode. This explains why the highest frequency Raman mode does not appear in IR or dielectric experiments, since such experiments only report the transverse response. We show that the transverse counterpart also exhibits dispersion. We argue that these dispersive modes are due to optical phonons that travel along the H-bond network of water. Our results indicate that not only does water exhibit LO-TO splitting, but also that its dependence with temperature is anomalous. We suggest that this measurement provides an alternative probe to evaluate structural changes in liquid water as a function of temperature.

I. RESULTS

As in our previous work³³ we compared results from a rigid (TIP4P/ ϵ) model, a flexible model (TIP4P/2005f), and a flexible and polarizable model (TTM3F) in all of our analyses.

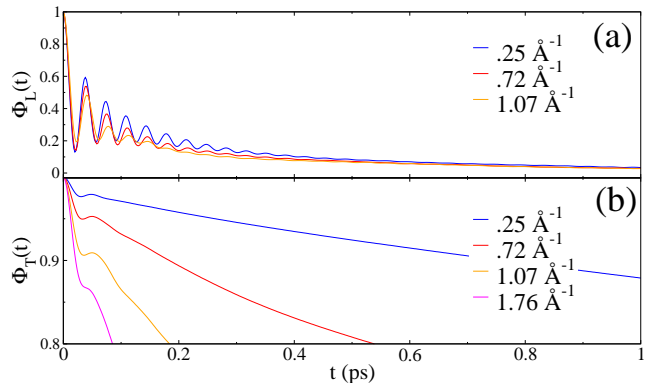


FIG. 2. **Polarization correlation functions.** Longitudinal (a) and transverse (b) polarization correlation functions (see equation 7) for TIP4P/ ϵ , a rigid model. The oscillations at small k come from the collective librational mode, which is much more pronounced in the longitudinal case.

II. LO-TO SPLITTING FROM EXPERIMENTAL DATA

We wish to study the k dependence of the dielectric susceptibility, where $k = 2\pi/\lambda$. k -dependence cannot be probed directly by experiment, but in the limit of infinite wavelength ($k \rightarrow 0$) the longitudinal and transverse dielectric susceptibilities can be obtained from the dielectric function via the following relations:^{34,35}

$$\chi_L(k \rightarrow 0, \omega) = 1 - \frac{1}{\epsilon(\omega)} \quad (4)$$

$$\chi_T(k \rightarrow 0, \omega) = \epsilon(\omega) - 1 \quad (5)$$

Note that the transverse susceptibility is what one normally calls susceptibility. The dielectric function can be obtained from the index of refraction $n(\omega)$ and extinction coefficient $k(\omega)$ as:

$$\begin{aligned} \epsilon'(\omega) &= n^2(\omega) - k^2(\omega) \\ \epsilon''(\omega) &= 2n(\omega)k(\omega) \end{aligned} \quad (6)$$

These equations allow us to use previously published experimental data^{31,32} to calculate the imaginary part of the longitudinal response. We find significant LO-TO splitting in the librational and stretching bands (fig. 1).

A. Polarization correlation functions

The normalized longitudinal and transverse polarization correlation functions are defined as:

$$\Phi_{L/T}(k, t) \equiv \frac{\langle \mathbf{P}_{L/T}(k, t) \cdot \mathbf{P}_{L/T}^*(k, 0) \rangle}{\langle \mathbf{P}_{L/T}(k, 0) \cdot \mathbf{P}_{L/T}^*(k, 0) \rangle} \quad (7)$$

The correlation functions found for TIP4P/ ϵ at small k are shown in figure 2. Since TIP4P/ ϵ is a rigid

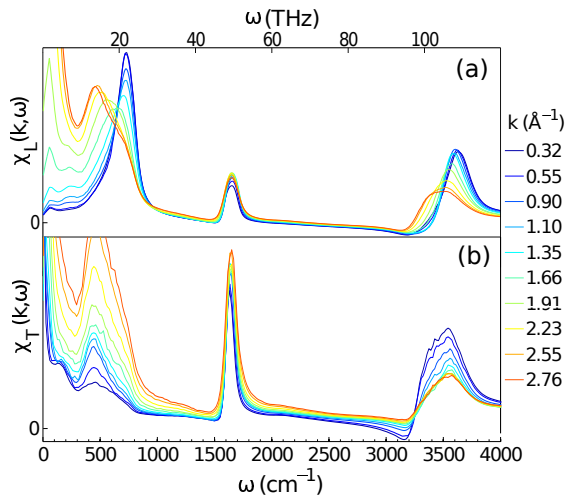


FIG. 3. **Imaginary part of longitudinal (a) & transverse (top) susceptibility** From a simulation with TTM3F at 300 K. In the longitudinal spectra both the librational ($\approx 750 \text{ cm}^{-1}$) and OH stretching peak ($\approx 3500 \text{ cm}^{-1}$) peaks exhibit dispersion.

Model	Temp	ω_{LO}	τ_{LO}	ω_{TO}	τ_{TO}	$\omega_{LO} - \omega_{TO}$
TIP4P/2005f	250	905	.38	667	.23	233
	300	900	.44	632	.18	268
	350	871	.34	574	.18	297
	400	826	.25	423	.17	400
TTM3F	250	757	.49	496		261
	300	721	.44	410		311
	350	710	.20	380		330
expt ³¹	253	820		641		179
expt ³²	300	759		556		203

TABLE I. **Resonance frequencies and lifetimes** Frequencies are given in cm^{-1} and lifetimes in picoseconds. The values from simulation were computed at the smallest k in the system. The experimental values are based on the position of the max of the band and therefore only approximate.

model, only librational motions are present. The addition of flexibility and polarizability add additional high frequency oscillations to the picture (Supplementary Fig. 1). In the small wavenumber regime ($k < 1.75 \text{ \AA}^{-1}$) there is a damped oscillation which corresponds to the collective librational phonon-like mode. This damped oscillation is superimposed on an underlying exponential relaxation in both the transverse and longitudinal cases. In the longitudinal case the relaxation time $\tau(k)$ of the underlying exponential relaxation exhibits non-monotonic behaviour with k , reaching a maximum at $k \approx 3 \text{ \AA}^{-1}$ (Supplementary Fig. 2). At wavenumbers greater than $k \approx 2.5 \text{ \AA}^{-1}$ only intramolecular motions contribute.

B. Dispersion of the librational peak

Figure 3 shows the imaginary part of the longitudinal and transverse susceptibility for TTM3F. In the longitudinal case the librational peak is clearly seen to shift with k . In the transverse case, the lower frequency portion of the band is seen to shift slightly with k . Dispersion relations for the longitudinal and transverse librational peaks are shown in figure 5 for three different temperatures, using one peak fits. The dispersion relations appear to be that of optical phonons. In both the longitudinal and transverse case the dampening factors remain less than the resonance frequencies, indicating an underdamped oscillation (Supplementary Fig. 3). The longitudinal dispersion relation for TIP4P/2005f agrees with that found by Bopp & Kornyshev (who used the flexible BJH model).²¹ Resat et al. also obtained a similar dispersion relation (but at a higher frequency), using the reference memory function approximation for TIP4P instead of molecular dynamics.³⁶

Resonance frequencies and lifetimes for the smallest k are shown in table IIB. The speed of propagation of these modes was computed by finding the slope $d\omega/dk$ in the regime of linear dispersion. For TIP4P/2005f we found speeds of $\approx 2700 \text{ m/s}$ and $\approx 1800 \text{ m/s}$ for the longitudinal and transverse modes. These propagation speeds are above the speed of sound in water (1500 m/s) but below the speed of sound in ice (4000 m/s). The temperature dependence of the propagation speed was found to be very small.

In both the longitudinal and transverse cases, the residual of the peak fitting shows features not captured by our Debye + one resonance fit of the librational peak. In both the longitudinal and transverse cases there is a non-dispersive peak at higher frequency, located at $\approx 900 \text{ cm}^{-1}$ for TIP4P/2005f and at $\approx 650 \text{ cm}^{-1}$ in TTM3F. This peak is negligibly small in the $k = 0$ longitudinal susceptibility but appears as a shoulder as k increases. In the transverse case the overlapping peak persists at $k = 0$, so we found that the $k = 0$ transverse spectra is best fit with two peaks, in agreement with experimental spectra. As we describe later, the higher frequency transverse peak is largely due to the self part of the response and is associated with the wagging librations of single molecules.

C. Importance of polarizability

There are several notable differences between TTM3F and the non-polarizable model TIP4P/2005f. First of all, the librational band of TIP4P/2005f is at higher frequency, in worse agreement with experiment. This difference in frequency is likely related to the parameters of TIP4P/2005f and not its lack of polarization. More importantly, we find that TTM3F exhibits dispersion in the OH stretching band ($\approx 3500 \text{ cm}^{-1}$) in the longitudinal case while TIP4P/2005f does not. The transverse

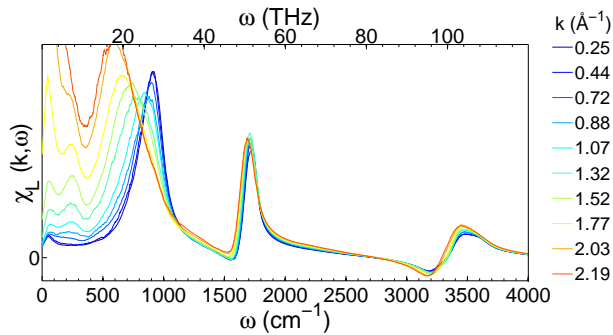


FIG. 4. **Imaginary part of the longitudinal susceptibility.** For TIP4P/2005f at 300 K. No significant dispersion is observed in the OH stretching peak.

susceptibility of TTM3F does not exhibit such dispersion but the magnitude of the OH stretching band increases at small k , indicating long range intermolecular correlations. TIP4P/2005f does not exhibit this behavior. Similarly, at $k = 0$ TTM3F exhibits significant LO-TO splitting in the OH stretching band while TIP4P/2005f does not (fig. 6). These findings are consistent with Heyden et al.’s results for the k -resolved IR spectra from ab-initio simulation, where they concluded that polarization allows for intermolecular correlations at the OH-stretch frequency.³⁷

These findings can be understood from the dipole derivative in equation 3. In the librational band the derivative of the dipole moment with respect to normal coordinate is purely due to rotation, while in the OH-stretching band it is due to changes in the geometry of the molecule and electronic polarization of the molecule during the OH stretching. In principle there may be coupling between the librational and stretching motions, but typically such rotational-vibrational coupling effects are negligibly small.³⁸ The dipole moment surface (fluctuating charges) and polarization dipole incorporated in TTM3F account for the changes in polarization that occur during OH stretching motion. These results confirm the significance of polarization in capturing the OH stretching response of water.³⁷

Figure 6 shows a comparison of TTM3F, TIP4P/2005f and experiment at $k = 0$. While the location of the peaks in TTM3F are in good agreement with the experimental data at 298 K, the magnitude of the longitudinal response is greatly overestimated in TTM3F. The degree of LO-TO splitting in the OH stretching peak is also overestimated in TTM3F. In general it appears that TTM3F overestimates the dipole derivative in equation 3 while TIP4P/2005f underestimates it. Figure 6 also shows the effect of polarization at low frequencies, in particular the appearance of an H-bond stretching response at $\approx 250 \text{ cm}^{-1}$ in TTM3F which is absent in TIP4P/2005f.³³

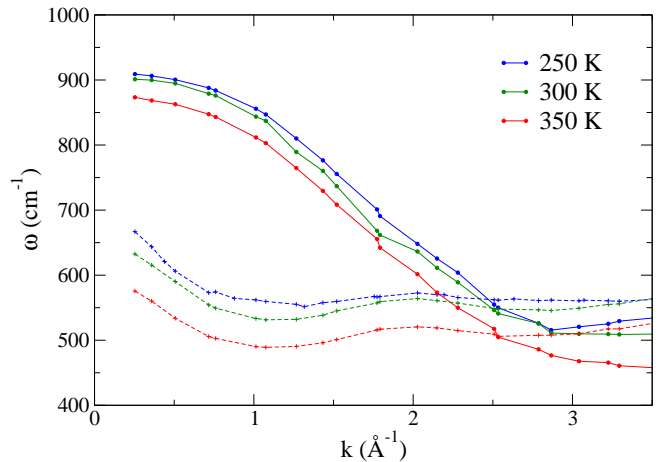


FIG. 5. **Dispersion relations for the propagating librational modes.** For TIP4P/2005f at three different temperatures (squares = longitudinal, pluses = transverse). A similar plot was found for TTM3F, but with lower frequencies.

D. LO-TO splitting vs temperature

The frequencies of the librational and stretching modes are shown in table II B. Once again we compare our results to experimental data.^{31,32,39} The comparison is imperfect since the TIP4P/2005f and TTM3F data comes from data at finite k (the smallest k in the system). For all three systems (TIP4P/2005f, TTM3F, and experiment) the increase in the LO-TO splitting of the librational band is puzzling, since the right hand side of the LST relation predicts a decrease in splitting, corresponding to a smaller dielectric constant and weaker dipole-dipole interactions. We found verifying the generalized LST equation is difficult because water contains either two or three Debye relaxations which must be taken into account.^{40,41} Uncertainties in how to fit the region of 1 - 300 cm^{-1} (.2- 9 THz), which includes contributions from many H-bonding modes, precludes a direct application of the generalized LST relation to water. By ignoring this region, however, we were able to achieve an approximate validation of the generalized LST equation for TIP4P/2005f. A more detailed analysis of how to fit the low frequency region will be the focus of future work. Since the generalized LST equation is an exact sum rule it can be used to assist in testing the validity of different fit functions.

E. Relation to phonons in ice

Naturally we would like to find corresponding optical phonon modes in ice. As shown in figure 1 the dielectric spectra and LO-TO splitting of supercooled water resembles that of ice. Recently evidence has been presented for propagating librational phonon modes in ice XI.^{42,43} Three of the twelve librational modes of ice XI

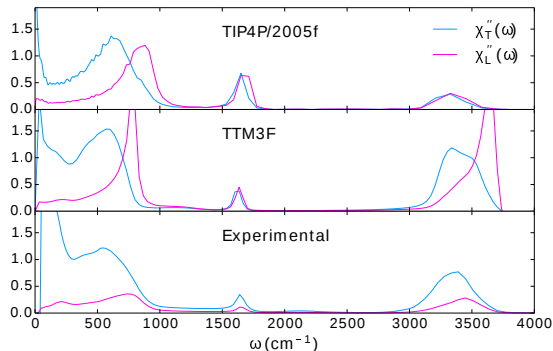


FIG. 6. **Imaginary parts of dielectric susceptibility.** We compare (a) the non-polarizable model TIP4P/2005f, (b) the polarizable model TTM3F, and (c) experimental data³² at 298 K. The effects of polarization can be seen in the LO-TO splitting of the stretching mode and in the low frequency features.

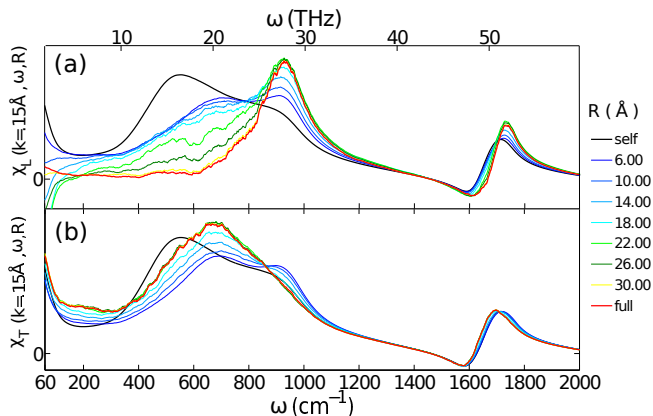


FIG. 7. **Imaginary part of the distance decomposed susceptibility for TIP4P/2005f.** Transverse (a) and longitudinal (b) susceptibilities, calculated with a 4 nm box at 300K, using the smallest k vector in the system. Gaussian smoothing was applied. Long range contributions to the librational peak extending to $R = 2$ nm are observed.

are IR active (labeled WR1, RW1 and RW2) and all three exhibit LO-TO splitting. The splittings have been found from Raman scattering to be 255, 135 and 35 cm^{-1} .⁴³ These modes all consist of coupled wagging and rocking motions. The WR1 mode, which has the largest infrared intensity, most closely matches our results. WR1 and RW2 have the same transverse frequency and RW1 has a smaller infrared intensity, which may help explain why the librational band is well fit by a single optical mode. LO-TO splitting in the OH-stretching modes of ice Ih has been discussed previously.¹⁷

F. Range of propagation

The range of propagation of these modes can be calculated as $R = \tau v_g$ where τ is the lifetime and $v_g = d\omega/dk$ is the group velocity. For TIP4P/2005f we find a range of propagation of ≈ 1.1 nm for the longitudinal librational mode and $\approx .3$ nm for the transverse mode. Similar results hold for TTM3F.

To verify that the modes we observe are actually propagating and to further quantify the range of propagation we study the spatial extent of polarization dipole correlations as a function of frequency. We investigated several different methodologies that can be used to decompose a spectra into distance-dependent components (Supplementary Note 1). We choose to start with the polarization correlation function:

$$\phi(k, t) = \left\langle \sum_i \mathbf{p}_i(k, 0) \cdot \sum_j \mathbf{p}_j(k, t) \right\rangle \quad (8)$$

Here $\mathbf{p}_i(k, t)$ represents either the longitudinal or transverse molecular polarization vector of molecule i . We now limit the molecules in the second sum to those in a sphere of radius R around each molecule i :

$$\phi(k, t, R) = \left\langle \sum_i \mathbf{p}_i(k, 0) \cdot \sum_{j \in R_i} \mathbf{p}_j(k, t) \right\rangle \quad (9)$$

The resulting function exhibits the expected $R \rightarrow 0$ limit, yielding only the self contribution. R can be increased to the largest R in the system ($\sqrt{3}L/2$), where the full response function for the simulation box is recovered. As R increases, the contributions of the distinct term add constructively and destructively to the self term, illustrating the contributions from molecules at different distances.

Figure 7 shows the distance decomposed longitudinal and transverse susceptibilities for TIP4P/2005f in a 4 nm box at the smallest k available in the system. The entire region between 0 - 1000 cm^{-1} contains significant cancellation between the self and distinct parts, in qualitative agreement with a previous study.⁴⁴ In the longitudinal susceptibility, the self component has two peaks (at 500 and 900 cm^{-1} for TIP4P/2005f) representing the two IR active librational motions (rocking and wagging, respectively). The self part is the same in both the longitudinal and transverse cases, reflecting an underlying isotropy which is only broken when dipole-dipole correlations are introduced. Further insight into the self-distinct cancellation comes from the results of Bopp, et. al., who project the hydrogen currents into a local molecular frame, allowing them to study the cross correlations between the rocking and wagging librations.²¹ They find that in the longitudinal case cross correlations between rocking and wagging contribute negatively in the region of 480 cm^{-1} and positively in the region of 740 cm^{-1} , suppressing the lower frequency peak to zero and enhancing the higher frequency peak.

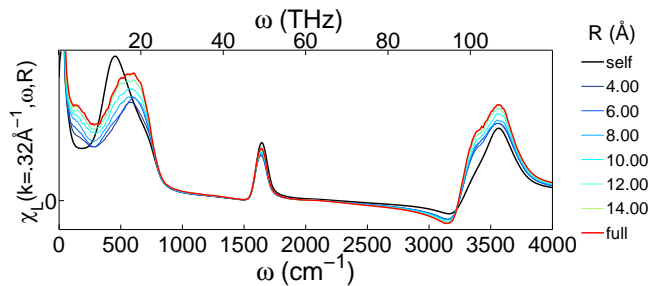


FIG. 8. Imaginary part of the distance decomposed longitudinal susceptibility for TTM3F at 300 K. Long range contributions are observed in the OH stretching band.

In both the transverse and longitudinal cases as R increases a new peak emerges, corresponding to the propagating mode. Incidentally, the shift in the peak between the self and distinct parts rules out the possibility that the propagating mode is the proposed dipolar plasmon resonance since the dipolar plasmon must be a resonance of both the of single molecule and collective motion.^{45–47} Interestingly, there are very long range contributions to this peak. In our simulations with a 4 nm box of TIP4P/2005f contributions persist up to 3 nm in the longitudinal case and 2 nm in the transverse case. As noted, recent studies of ice XI suggest that the propagating modes consist of coupled wagging and rocking librations.^{42,43} The results for the transverse mode seem to confirm this hypothesis for liquid water, since the propagating mode peak lies between the single molecule rocking and wagging peaks. In the longitudinal case the propagating mode overlaps more with the wagging peak, suggesting a greater role for these type of librations in the longitudinal phonon.

G. Methanol & acetonitrile

To provide further evidence the aforementioned optical modes propagate through the hydrogen bond network of water we decided to repeat our analysis for other polar liquids, both H-bonding and non H-bonding. As an H-bonding liquid we choose methanol, which is known to contain winding H-bonded chains. According to results from MD simulation, most of these chains have around 5-6 molecules^{48,49}, with a small percentage of chains containing 10-20 molecules.⁵⁰ Chain lifetimes have been estimated to be about .5 ps.⁵⁰ Therefore we expect methanol can also support a librational phonon mode that propagates along hydrogen bonds, but perhaps with a shorter lifetime and range than water. As a non H-bonding polar liquid we choose acetonitrile, because it has a structure similar to methanol, but with the hydroxyl group replaced by a carbon atom. We find that the OH librational band of methanol ($\approx 700 \text{ cm}^{-1}$) is indeed dispersive (Supplementary Fig. 4). As with water, the transverse spectra also exhibits dispersion, but to a much

lesser extent. LO-TO splitting of about 100 cm^{-1} is observed in the 700 cm^{-1} librational peak. The results for acetonitrile are more ambiguous - we observe dispersion in the broad peak at $\approx 100 \text{ cm}^{-1}$, however this peak contains contributions from translational and (free) rotational modes, as well as the CH_3 torsion mode, and it is not clear which modes are responsible for the dispersion (Supplementary Fig. 5).

III. DISCUSSION

In this work we have presented several lines of evidence for short lived optical phonons that propagate along the H-bond network of water. The longitudinal and transverse nonlocal susceptibility exhibit dispersive peaks with dispersion relations resembling optical phonons. As the temperature is lowered, the resonance frequencies and LO-TO splittings of these modes converge towards the values for phonons in ice Ih. By comparing our results with a recent study of ice XI we believe both modes likely consist of coupled wagging and rocking librations.^{42,43}

This work fundamentally changes our understanding of the librational band in the Raman spectra of water by assigning the lower and higher frequency peaks to transverse and longitudinal optical modes. Our analysis of the self-distinct cancellation indicates that the middle Raman peak ($\approx 600 \text{ cm}^{-1}$) belongs to the remnant of the single molecule wagging response which remains after the cancellation. We are also led to a new interpretation the librational region of the real part of the dielectric function. In the case of a lossless optical phonon the transverse phonon occurs where $\epsilon'(\omega) = \infty$ while the longitudinal phonon occurs where $\epsilon'(\omega) = 0$. The presence of dampening smooths the divergence leading to a peak followed by a sharp dip. This is what is observed in the real part of the dielectric function of water between $300 - 500 \text{ cm}^{-1}$ (the features are shifted to lower frequencies by the tail of the low frequency Debye relaxation).

One might wonder how our work relates to existing work on acoustic modes in water, in particular, the controversial “fast sound” mode.^{52,53} Acoustic modes, which are observable through the dynamic structure factor, have been explored as means of understanding the hydrogen bond structure and low temperature anomalies of water.⁵ In this work we have argued that optical modes can also provide insight into water’s structure and dynamics. The fast sound mode lies at much lower frequencies than the librational and OH stretch modes that we studied. The H-bond bending and stretching modes also primarily lie at frequencies below the librational region. However, normal mode analysis of liquid water and clusters shows that the H-bond stretching modes have a wide distribution of frequencies which overlaps with the librational modes, so some coupling between these modes is possible.^{54,55} Recently it was shown that there is coupling between the acoustic and optic modes in water - ie. between fluctuations in mass density and fluctuations in

charge density.⁵⁶

The large spatial range and coherent propagation of these modes is surprising and implies the existence of an extended hydrogen bond network, in contrast to earlier ideas about the structure of water which emphasize dynamics as being confined within small clusters.⁵⁷ Simulations with larger simulation boxes are needed to fully quantify the extent of the longitudinal modes. The ability of water to transmit phonon modes may be relevant to biophysics, where such modes could lead to dynamical coupling between biomolecules, a phenomena which is currently only being considered at much lower frequencies.⁵⁸⁻⁶⁰ The methodology used in this paper to analyse LO-TO splitting opens up a new avenue to understanding the structure and dynamics of water. The fact that the librational LO-TO splitting increases with temperature instead of the expected decrease is likely due to significant changes in the structure of the liquid. One likely possibility is that the volume per ‘‘unit cell’’ term in equation 3 decreases with temperature. This could be caused by the local quasi-structure determined by H-bonding changing from a more ice-like structure (4 molecules per unit cell) to a more cubic structure (1 molecule per unit cell). More research is needed to understand the microscopic origin of the LO-TO splitting in water, both in the librational and stretching modes.

IV. METHODS

A. Theory of the nonlocal susceptibility

If the external field is sufficiently small, the relation between the polarization response of a medium and the electric displacement field \mathbf{D} for a spatially homogeneous system is given by :

$$\mathbf{P}(\mathbf{r}, t) = \epsilon_0 \int_V \int_{-\infty}^t d\mathbf{r}' dt' \overset{\leftrightarrow}{\chi}(\mathbf{r} - \mathbf{r}', t - t') \mathbf{D}(\mathbf{r}', t') \quad (10)$$

This expression Fourier transforms to:

$$\mathbf{P}(\mathbf{k}, \omega) = \epsilon_0 \overset{\leftrightarrow}{\chi}(\mathbf{k}, \omega) \mathbf{D}(\mathbf{k}, \omega) \quad (11)$$

For isotropic systems, the tensor $\overset{\leftrightarrow}{\chi}$ can be decomposed into longitudinal and transverse components:

$$\overset{\leftrightarrow}{\chi}(\mathbf{k}, \omega) = \chi_L(k, \omega) \hat{\mathbf{k}} \hat{\mathbf{k}} + \chi_T(k, \omega) (\mathbf{I} - \hat{\mathbf{k}} \hat{\mathbf{k}}) \quad (12)$$

The easiest starting point for deriving microscopic expressions for $\chi_L(k, \omega)$ and $\chi_T(k, \omega)$ is the classical Kubo formula:⁶¹

$$\chi_{L/T}(\mathbf{k}, \omega) = \frac{\beta}{\epsilon_0} \int_0^\infty dt \frac{d}{dt} \langle \mathbf{P}_{L/T}(\mathbf{k}, t) \cdot \mathbf{P}_{L/T}^*(\mathbf{k}, 0) \rangle e^{i\omega t} \quad (13)$$

This expression relates the susceptibility to the time correlation function of the polarization in equilibrium.

The longitudinal part of the polarization can be calculated by Fourier transforming the defining expression for the polarization $\nabla \cdot \mathbf{P}(\mathbf{r}, t) = -\rho(\mathbf{r}, t)$, leading to $\hat{\mathbf{k}} \cdot \mathbf{P} = i\rho(\mathbf{k}, t)/k = P_L$. To calculate the transverse part of the polarization we use the method of Raineri & Friedman to find the polarization vector of each molecule (Supplementary Note 2).⁶² We can rewrite eqn. 13 in terms of the normalized polarization correlation function (eqn. 7), and taking into account the isotropy of water:

$$\chi_{L/T}(k, \omega) = \chi_{L/T}(k, 0) \int_0^\infty \dot{\Phi}_{L/T}(k, t) e^{i\omega t} dt \quad (14)$$

B. Computational methods

The three water models we used were TIP4P/ ϵ ,⁶³ TIP4P/2005f,⁶⁴ and TTM3F.⁶⁵ To simulate methanol and acetonitrile we used the General AMBER Forcefield (GAFF),⁶⁶ a forcefield with full intramolecular flexibility which has been shown to satisfactorily reproduce key properties of both liquids.⁶⁷ Our TTM3F simulations were performed with an in-house code that uses the TTM3F force calculation routine of Fanourgakis and Xantheas. All other simulations were ran using the GRO-MACS package (ver. 4.6.5).⁶⁸ We used particle-mesh Ewald summation for the long range electrostatics with a Coloumb cutoff of 2 nm for our 4+ nm simulations and a cutoff of 1.2 nm for our simulations with 512 molecules. Our TTM3F simulations had 256 molecules and used Ewald summation with a Coulomb cutoff of .9 nm. The principle TIP4P/2005f simulations contained 512 molecules and were 8 ns long ($\Delta t_{\text{out}} = 8$ fs) and .6 - 1.2 ns long ($\Delta t_{\text{out}} = 4$ fs). Other simulations were 1-2 ns long. Simulations with MeOH and ACN contained 1,000 molecules and were 1 ns long. All simulations were equilibrated for at least 50 ps prior to outputting data.

Because of periodic boundary conditions, the possible \mathbf{k} vectors are limited to the form $\mathbf{k} = 2\pi n_x \hat{\mathbf{i}}/L_x + 2\pi n_y \hat{\mathbf{j}}/L_y + 2\pi n_z \hat{\mathbf{k}}/L_z$, where n_x , n_y , and n_z are integers. We calculated correlation functions separately for each \mathbf{k} and then average over the results for \mathbf{k} vectors with the same magnitude, a process we found reduced random noise.

One can question whether a purely classical treatment is justified here because the librational dynamics we are interested have frequencies of 700-900 cm^{-1} for which $\hbar\omega \approx 3 - 4k_B T$ at 300 K. Previously it was shown that the widely-used harmonic correction does not change the spectrum.²¹ Furthermore, comparison of k resolved IR spectra taken from molecular dynamics and ab-initio DFT simulation show that they give qualitatively similar results for all frequencies below 800 cm^{-1} .³⁷ For the OH stretching peak, however, quantum effects are known to be very important.

C. Fitting the librational band

To obtain resonance frequencies and lifetimes for the librational peak in the imaginary part of the response we used a damped oscillator model. A Debye peak overlaps significantly with the librational band in both the longitudinal and transverse cases and must be included in the peak fitting. Equation 14 can be used to relate the form of the time correlation function to the absorption peak lineshape. For Debye response one has the following expressions:

$$\begin{aligned}\Phi(k, t) &= Ae^{-t/\tau_D} \\ \frac{\text{Im}\{\chi(k, \omega)\}}{\chi(k, 0)} &= \frac{A\omega\tau_D}{1 + \omega^2\tau_D^2}\end{aligned}\quad (15)$$

For resonant response with resonance frequency $\omega_0(k)$ and dampening factor $\gamma \equiv 1/\tau$ we have:

$$\begin{aligned}\Phi(k, t) &= Be^{-t/\tau} \cos(\omega_0 t) \\ \frac{\text{Im}\{\chi(k, \omega)\}}{\chi(k, 0)} &= \frac{B}{2} \left(\frac{\omega\tau}{1 + (\omega + \omega_0)^2\tau^2} + \frac{\omega\tau}{1 + (\omega - \omega_0)^2\tau^2} \right)\end{aligned}$$

We find this lineshape (the Van Vleck-Weisskopf lineshape^{69,70}) yields results identical to the standard damped harmonic oscillator response for the range of τ, ω_0 values we are interested in. We found a two function (Debye + resonant) fit worked very well for fitting the librational peak in the longitudinal case (Supplementary Figs. 7 and 8). The H-bond stretching peak at $\approx 200 \text{ cm}^{-1}$ overlaps with the librational band for $2 < k < 2.5$, and we found that it can be included in the fit using an additional damped harmonic oscillator, but usually this was not necessary. Because of this overlap and due to the broad nature of the transverse band, the fitting in the transverse case is only approximate. We found this was especially true for TTM3F and the experimental data, so we do not report lifetimes for such cases.

V. ACKNOWLEDGMENTS

This work was partially supported by DOE Award No. DE-FG02-09ER16052 (D.C.E.) and by DOE Early Career Award No. DE-SC0003871 (M.V.F.S.).

REFERENCES

- ¹Santra, B., Jr., R. A. D., Martelli, F. & Car, R. Local structure analysis in ab initio liquid water. *Mol. Phys.* 1–13 (in press 2015).
- ²Errington, J. R. & Debenedetti, P. G. Relationship between structural order and the anomalies of liquid water. *Nature* **409**, 318–321 (2001).
- ³English, N. J. & Tse, J. S. Density fluctuations in liquid water. *Phys. Rev. Lett.* **106**, 037801 (2011).
- ⁴Huang, C. *et al.* The inhomogeneous structure of water at ambient conditions **106**, 15214–15218 (2009).
- ⁵Mallamace, F., Corsaro, C. & Stanley, H. E. Possible relation of water structural relaxation to water anomalies. *Proc. Natl. Acad. Sci. USA* **110**, 4899–4904 (2013).
- ⁶Sahle, C. J. *et al.* Microscopic structure of water at elevated pressures and temperatures. *Proc. Natl. Acad. Sci. USA* **110**, 6301–6306 (2013).
- ⁷Walrafen, G. E. Raman spectral studies of water structure. *J. Phys. Chem.* **40**, 3249 (1964).
- ⁸Carey, D. M. & Korenowski, G. M. Measurement of the Raman spectrum of liquid water. *J. Chem. Phys.* **108**, 2669–2675 (1998).
- ⁹Walrafen, G. E. Raman spectrum of water: transverse and longitudinal acoustic modes below $\approx 300 \text{ cm}^{-1}$ and optic modes above $\approx 300 \text{ cm}^{-1}$. *J. Phys. Chem.* **94**, 2237–2239 (1990).
- ¹⁰Walrafen, G. E. Raman spectral studies of the effects of temperature on water structure. *J. Phys. Chem.* **47**, 114–126 (1967).
- ¹¹Walrafen, G. E., Fisher, M. R., Hokmabadi, M. S. & Yang, W. Temperature dependence of the low and high-frequency Raman scattering from liquid water. *J. Chem. Phys.* **85**, 6970–6982 (1986).
- ¹²Castner, E. W., Chang, Y. J., Chu, Y. C. & Walrafen, G. E. The intermolecular dynamics of liquid water. *J. Chem. Phys.* **102**, 653–659 (1995).
- ¹³Zelmann, H. R. Temperature dependence of the optical constants for liquid H₂O and D₂O in the far IR region. *J. Mol. Str.* **350**, 95–114 (1995).
- ¹⁴Fukasawa, T. *et al.* Relation between dielectric and low-frequency Raman spectra of hydrogen-bond liquids. *Phys. Rev. Lett.* **95**, 197802 (2005).
- ¹⁵Aure, P. & Chosson, A. The translational lattice-vibration Raman spectrum of single crystal ice 1h. *J. Glaciology* **21**, 65–71 (1978).
- ¹⁶Klug, D. D., Tse, J. S. & Whalley, E. The longitudinal-optic-transverse-optic mode splitting in ice 1h. *J. Chem. Phys.* **95**, 7011–7012 (1991).
- ¹⁷Whalley, E. A detailed assignment of the oh stretching bands of ice i. *Canadian Journal of Chemistry* **55**, 3429–3441 (1977).
- ¹⁸Klug, D. D. & Whalley, E. Origin of the high-frequency translational bands of ice i*. *J. Glaciology* **21**, 55–63 (1978).
- ¹⁹Galeener, F. L. & Lucovsky, G. Longitudinal optical vibrations in glasses: GeO₂ and SiO₂. *Phys. Rev. Lett.* **37**, 1474–1478 (1976).
- ²⁰Resat, H., Raineri, F. O. & Friedman, H. L. Studies of the optical like high frequency dispersion mode in liquid water. *J. Chem. Phys.* **98**, 7277 (1993).
- ²¹Bopp, P. A., Kornyshev, A. A. & Sutmann, G. Frequency and wave-vector dependent dielectric function of water: Collective modes and relaxation spectra. *J. Chem. Phys.* **109**, 1939 (1998).
- ²²Ricci, M. A., Rocca, D., Ruocco, G. & Vallauri, R. Theoretical and computer-simulation study of the density fluctuations in liquid water. *Phys. Rev. A* **40**, 7226–7238 (1989).
- ²³Lyddane, R. H., Sachs, R. G. & Teller, E. On the polar vibrations of alkali halides. *Phys. Rev.* **59**, 673–676 (1941).
- ²⁴Barker, A. S. Long-wavelength soft modes, central peaks, and the Lyddane-Sachs-Teller relation. *Phys. Rev. B* **12**, 4071–4084 (1975).
- ²⁵Sievers, A. J. & Page, J. B. Generalized Lyddane-Sachs-Teller relation and disordered solids. *Phys. Rev. B* **41**, 3455–3459 (1990).
- ²⁶Payne, M. & Inkson, J. Longitudinal-optic-transverse-optic vibrational mode splittings in tetrahedral network glasses. *Journal of Non-Crystalline Solids* **68**, 351 – 360 (1984).
- ²⁷Sekimoto, K. & Matsubara, T. To-lo splittings of glassy dielectrics. *Phys. Rev. B* **26**, 3411 (1982).
- ²⁸Decius, J. C. & Hexter, R. M. *Molecular Vibrations in Crystals* (McGraw-Hill, USA, 1977).
- ²⁹Decius, J. C. Dipolar coupling and molecular vibration in crystals. i. general theory. *J. Chem. Phys.* **49**, 1387–1392 (1968).
- ³⁰Burba, C. M. & Frech, R. Existence of optical phonons in the room temperature ionic liquid 1-ethyl-3-methylimidazolium trifluoromethanesulfonate. *J. Chem. Phys.* **134**, 134503 (2011).
- ³¹Zasetsky, A. Y., Khalizov, A. F., Earle, M. E. & Sloan, J. J. Frequency dependent complex refractive indices of supercooled

- liquid water and ice determined from aerosol extinction spectra. *The Journal of Physical Chemistry A* **109**, 2760 (2005).
- ³²Hale, G. & Querry, M. Optical constants of water in the 200-nm to 200- μ m wavelength region. *Appl. Opt.* **12**, 555 (1973).
- ³³Elton, D. C. & Fernández-Serra, M.-V. Polar nanoregions in water: A study of the dielectric properties of TIP4P/2005, TIP4P/2005f and TTM3F. *J. Chem. Phys.* **140**, 124504 (2014).
- ³⁴Madden, P. & Kivelson, D. A consistent molecular treatment of dielectric phenomena. In *Adv. Chem. Phys.*, 467 (John Wiley & Sons, Inc., 2007).
- ³⁵Hansen, J.-P. & McDonald, I. R. Chapter 11 - molecular liquids. In Hansen, J.-P. & McDonald, I. R. (eds.) *Theory of Simple Liquids*, 341 (Academic Press, 2006), 3rd edn.
- ³⁶Resat, H., Raineri, F. O. & Friedman, H. L. A dielectric theory of the optically like high-frequency mode in liquid water. *J. Chem. Phys.* **97**, 2618 (1992).
- ³⁷Heyden, M. *et al.* Understanding the origins of dipolar couplings and correlated motion in the vibrational spectrum of water. *J. Phys. Chem. Lett.* **3**, 2135–2140 (2012).
- ³⁸Woodward, L. *Introduction to the theory of molecular vibrations and vibrational spectroscopy* (Clarendon Press, 1972).
- ³⁹Wagner, R. *et al.* Mid-infrared extinction spectra and optical constants of supercooled water droplets. *J. Phys. Chem. A* **109**, 7099–7112 (2005).
- ⁴⁰Vinh, N. Q. *et al.* High-precision gigahertz-to-terahertz spectroscopy of aqueous salt solutions as a probe of the femtosecond-to-picosecond dynamics of liquid water. *J. Chem. Phys.* **142**.
- ⁴¹Ellison, W. J. Permittivity of pure water, at standard atmospheric pressure, over the frequency range 0–25 THz and the temperature range 0100c. *J. Phys. Chem. Ref. D at.* **36**, 1–18 (2007).
- ⁴²Iwano, K., Yokoo, T., Oguro, M. & Ikeda, S. Propagating librations in ice xi: Model analysis and coherent inelastic neutron scattering experiment. *Journal of the Physical Society of Japan* **79**, 063601 (2010).
- ⁴³Shigenari, T. & Abe, K. Vibrational modes of hydrogens in the proton ordered phase XI of ice: Raman spectra above 400 cm^{-1} . *J. Chem. Phys.* **136** (2012).
- ⁴⁴Wan, Q., Spanu, L., Galli, G. A. & Gygi, F. Raman spectra of liquid water from ab initio molecular dynamics: Vibrational signatures of charge fluctuations in the hydrogen bond network. *Journal of Chemical Theory and Computation* **9**, 4124–4130 (2013).
- ⁴⁵Lobo, R., Robinson, J. E. & Rodriguez, S. High frequency dielectric response of dipolar liquids. *J. Chem. Phys.* **59**, 5992–6008 (1973).
- ⁴⁶Pollock, E. L. & Alder, B. J. Frequency-dependent dielectric response in polar liquids. *Phys. Rev. Lett.* **46**, 950–953 (1981).
- ⁴⁷Chandra, A. & Bagchi, B. Collective excitations in a dense dipolar liquid: How important are dipolarons in the polarization relaxation of common dipolar liquids? *J. Chem. Phys.* **92**, 6833 (1990).
- ⁴⁸Haughney, M., Ferrario, M. & McDonald, I. R. Molecular-dynamics simulation of liquid methanol. *The Journal of Physical Chemistry* **91**, 4934–4940 (1987).
- ⁴⁹Yamaguchi, T., Benmore, C. J. & Soper, A. K. The structure of subcritical and supercritical methanol by neutron diffraction, empirical potential structure refinement, and spherical harmonic analysis. *J. Chem. Phys.* **112**, 8976–8987 (2000).
- ⁵⁰Matsumoto, M. & Gubbins, K. E. Hydrogen bonding in liquid methanol. *J. Chem. Phys.* **93**, 1981–1994 (1990).
- ⁵¹Crowder, G. A. & Cook, B. R. Acetonitrile: far-infrared spectra and chemical thermodynamic properties. discussion of an entropy discrepancy. *The Journal of Physical Chemistry* **71**, 914–916 (1967).
- ⁵²Santucci, S. C., Fioretto, D., Comez, L., Gessini, A. & Masciovecchio, C. Is there any fast sound in water? *Phys. Rev. Lett.* **97**, 225701 (2006).
- ⁵³Sampoli, M., Ruocco, G. & Sette, F. Mixing of longitudinal and transverse dynamics in liquid water. *Phys. Rev. Lett.* **79**, 1678–1681 (1997).
- ⁵⁴Cho, M., Fleming, G. R., Saito, S., Ohmine, I. & Stratt, R. M. Instantaneous normal mode analysis of liquid water. *J. Chem. Phys.* **100**, 6672–6683 (1994).
- ⁵⁵Garberoglio, G., Vallauri, R. & Sutmann, G. Instantaneous normal mode analysis of correlated cluster motions in hydrogen bonded liquids. *J. Chem. Phys.* **117**, 3278–3288 (2002).
- ⁵⁶Sedlmeier, F., Shadkoo, S., Bruinsma, R. & Netz, R. R. Charge/mass dynamic structure factors of water and applications to dielectric friction and electroacoustic conversion. *J. Chem. Phys.* **140**, 054512 (2014).
- ⁵⁷Bosma, W. B., Fried, L. E. & Mukamel, S. Simulation of the intermolecular vibrational spectra of liquid water and water clusters. *J. Chem. Phys.* **98**, 4413–4421 (1993).
- ⁵⁸Conti Nibali, V. & Havenith, M. New insights into the role of water in biological function: Studying solvated biomolecules using terahertz absorption spectroscopy in conjunction with molecular dynamics simulations. *J. Am. Chem. Soc.* **136**, 12800 (2014).
- ⁵⁹Ebbinghaus, S. *et al.* An extended dynamical hydration shell around proteins. *Proc. Natl. Acad. Sci. USA* **104**, 20749 (2007).
- ⁶⁰Kim, S., Born, B., Havenith, M. & Gruebele, M. Real-time detection of protein-water dynamics upon protein folding by terahertz absorption spectroscopy. *Angewandte Chemie International Edition* **47**, 6486 (2008).
- ⁶¹Kubo, R. Statistical-mechanical theory of irreversible processes. i. general theory and simple applications to magnetic and conduction problems. *J. Phys. Soc. Jap.* **12**, 570–586 (1957).
- ⁶²Raineri, F. O. & Friedman, H. L. Static transverse dielectric function of model molecular fluids. *J. Chem. Phys.* **98**, 8910–8918 (1993).
- ⁶³Fuentes-Azcatl, R. & Alejandre, J. Non-polarizable force field of water based on the dielectric constant: TIP4P/ ϵ . *J. Phys. Chem. B* **118**, 1263–1272 (2014).
- ⁶⁴Gonzalez, M. A. & Abascal, J. L. F. A flexible model for water based on TIP4P/2005. *J. Chem. Phys.* **135**, 224516 (2011).
- ⁶⁵Fanourgakis, G. S. & Xantheas, S. S. Development of transferable interaction potentials for water. v. extension of the flexible, polarizable, thole-type model potential (TTM3-F, v. 3.0) to describe the vibrational spectra of water clusters and liquid water. *J. Chem. Phys.* **128**, 074506 (2008).
- ⁶⁶Wang, J. *et al.* Development and testing of a general AMBER force field. *J. Comput. Chem.* **25**, 1157 (2004).
- ⁶⁷Caleman, C. *et al.* Force field benchmark of organic liquids: Density, enthalpy of vaporization, heat capacities, surface tension, isothermal compressibility, volumetric expansion coefficient, and dielectric constant. *J. Chem. Theo. Comp.* **8**, 61 (2012).
- ⁶⁸Hess, B., Kutzner, C., van der Spoel, D. & Lindahl, E. GROMACS 4: Algorithms for highly efficient, load-balanced, and scalable molecular simulation. *J. Chem. Theo. Comp.* **4**, 435–447 (2008).
- ⁶⁹Toda, M., Kubo, R., Saitō, N. & Hashitsume, N. *Statistical Phys. II: Nonequilibrium Statistical Mechanics*. Series C (Springer Berlin Heidelberg, 1991).
- ⁷⁰Van Vleck, J. H. & Weisskopf, V. F. On the shape of collision-broadened lines. *Rev. Mod. Phys.* **17**, 227–236 (1945).
- ⁷¹Buchner, R., Barthel, J. & Stauber, J. The dielectric relaxation of water between 0c and 35c. *Chem. Phys. Lett.* **306**, 57 (1999).
- ⁷²Bolla, G. Su alcune nuove bande Raman dell'acqua. *Il Nuovo Cimento* **10**, 101–107 (1933).
- ⁷³Walrafen, G. E. Raman spectral studies of the effects of electrolytes on water. *J. Chem. Phys.* **36**, 1035–1042 (1962).
- ⁷⁴Heyden, M. *et al.* Dissecting the THz spectrum of liquid water from first principles via correlations in time and space. *Proc. Natl. Acad. Sci. USA* **107**, 12068–12073 (2010).
- ⁷⁵Bertolini, D. & Tani, A. The frequency and wavelength dependent dielectric permittivity of water. *Mol. Phys.* **75**, 1065–1088 (1992).
- ⁷⁶Bagchi, B. & Chandra, A. Molecular theory of underdamped dielectric relaxation: understanding collective effects in dipolar liquids. *Chem. Phys.* **173**, 133 – 141 (1993).

- ⁷⁷Ferraro, R. & Basile, L. *Fourier Transform Infrared Spectra: Applications to Chem. Systems*, vol. v. 1 (Elsevier Science, 1978).
- ⁷⁸Bagchi, B. & Chandra, A. Ultrafast solvation dynamics: Molecular explanation of computer simulation results in a simple dipolar solvent. *J. Chem. Phys.* **97** (1992).
- ⁷⁹Hill, N. E. The influence of the poley absorption on the inertial fall-off of the dielectric absorption. *J. Phys. C: Solid State Phys.* **4**, 2322 (1971).
- ⁸⁰Nora E. Hill, A. P. M. D., W. E. Vaughan. *Dielectric Properties and Molecular Behaviour* (Van Norstrand Reinhold Company, New York, 1963).
- ⁸¹Poley, J. Microwave dispersion of some polar liquids. *App. Sci. Res. B* **4**, 337–387 (1955).

VI. SUPPLEMENTARY INFORMATION

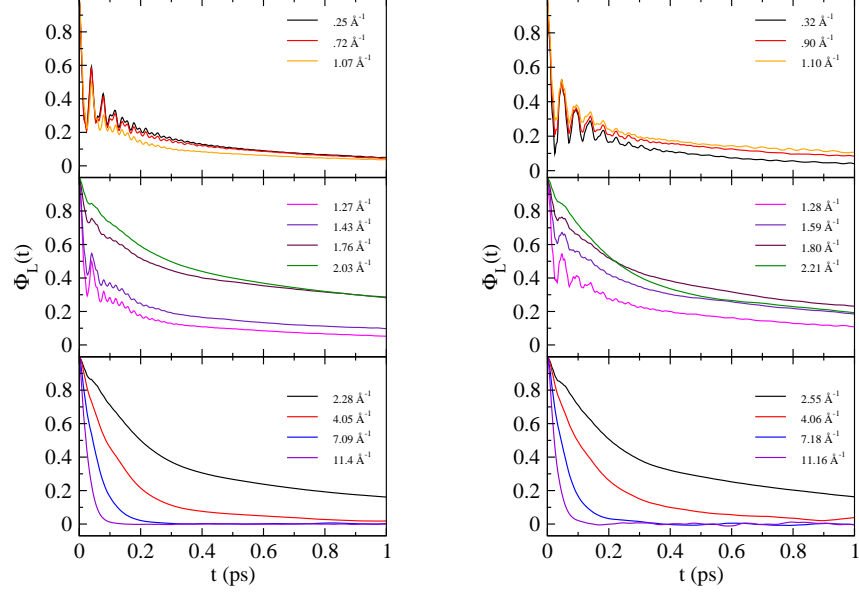


FIG. 1. Longitudinal polarization relaxation functions. Shown for 512 TIP4P2005/f (left) and TTM3F (right) at 300 K.

type	ω_{L1}	ω_{L2}	ω_{L3}	ref.
	510	—	780	Bolla (1933) ⁷²
	450	—	780	Walrafen (1962) ⁷³
	400	—	700	Fukasawa, et. al. (2005) ¹⁴
Raman	430	650	795	Carey, et. al. (1998) ⁸
	440	540	770	Castner, et. al. (1995) ¹²
	450	550	725	Walrafen (1990) ⁹
	424	550	725	Walrafen (1986) ¹¹
	439	538	717	Walrafen (1967) ¹⁰
infrared	380	665	—	Zelmann (1995) ¹³
dielectric	420	620	—	Fukasawa, et. al. (2005) ¹⁴

Supplementary Table 1: Experimental peaks in Raman, dielectric, and IR spectra. This table shows the correspondence between 3 peak Raman fits and 2 peak dielectric/IR fits to the librational region at 298 K.

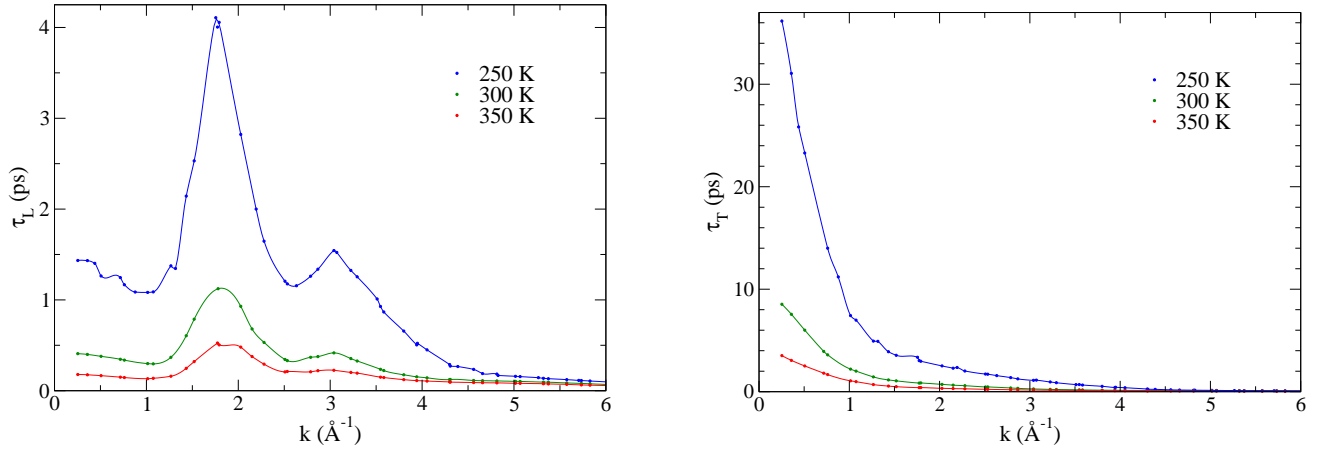


FIG. 2. **Longitudinal (left) and transverse (right) relaxation times for 512 TIP4P/2005f.** Computed for the underlying exponential of the relaxation. The points are interpolated by Akima splines. The transverse relaxation time here is equal to the Debye relaxation time, which at $k = 0$ is ≈ 11 ps at 300 K for TIP4P/2005f. Experimentally it is 8.5 ps.⁷¹

A. Supplementary info: Dispersion relations and dampening factors

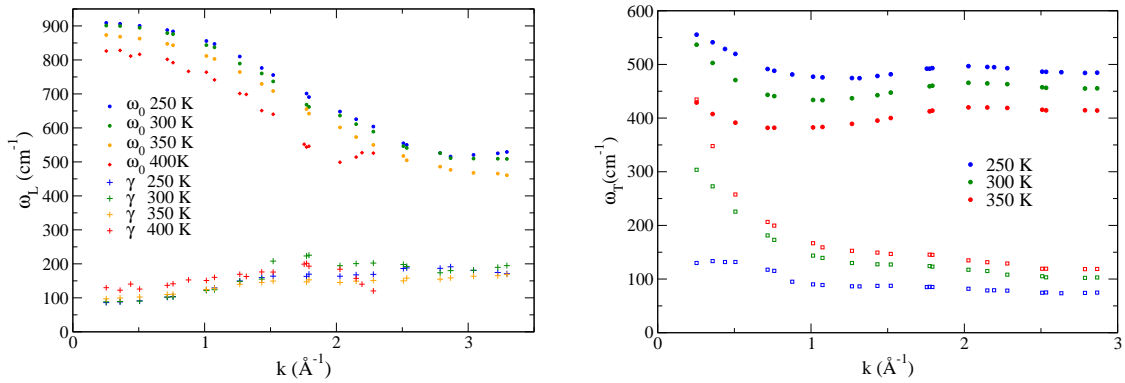


FIG. 3. **Longitudinal (left) and transverse (right) dispersion relations (circles) and dampening factors (squares) for 512 TIP4P/2005f.** These curves were obtained from a two peak (Debye + resonant) fit. In contrast to the longitudinal mode, the transverse mode is much more damped. However, the dampening factor changes significantly with temperature, also in contrast to the longitudinal case, and at 250 K becomes relatively small. Beyond 2 \AA^{-1} the peak due to the damped resonance starts to disappear so values beyond 3 \AA^{-1} are not shown.

VII. SUPPLEMENTARY INFO: METHANOL & ACETONITRILE

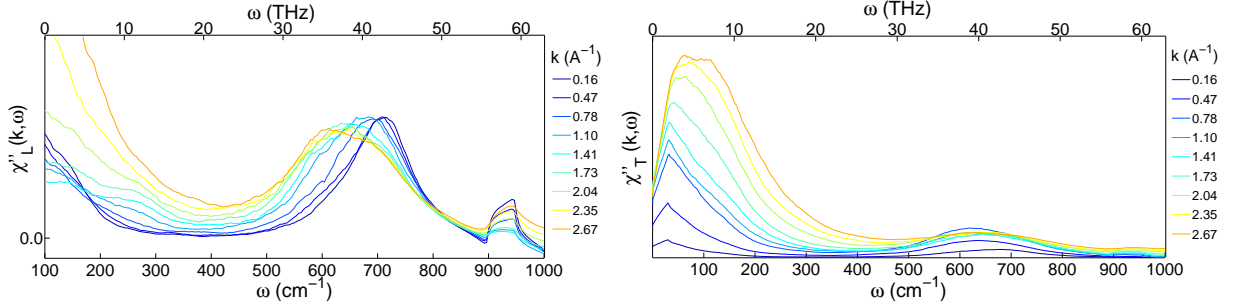


FIG. 4. **Longitudinal (left) and transverse (right) dielectric susceptibility for a system of 1,000 MeOH molecules.** The longitudinal librational peak at $\approx 700 \text{ cm}^{-1}$ clearly disperses with k , while the transverse peak at $\approx 600 \text{ cm}^{-1}$ disperses slightly with k . The higher frequency peaks exhibit no dispersion. The static dielectric function $\epsilon(k, 0)$ has not converged properly in the transverse case, so the magnitude of the peaks is not converged.

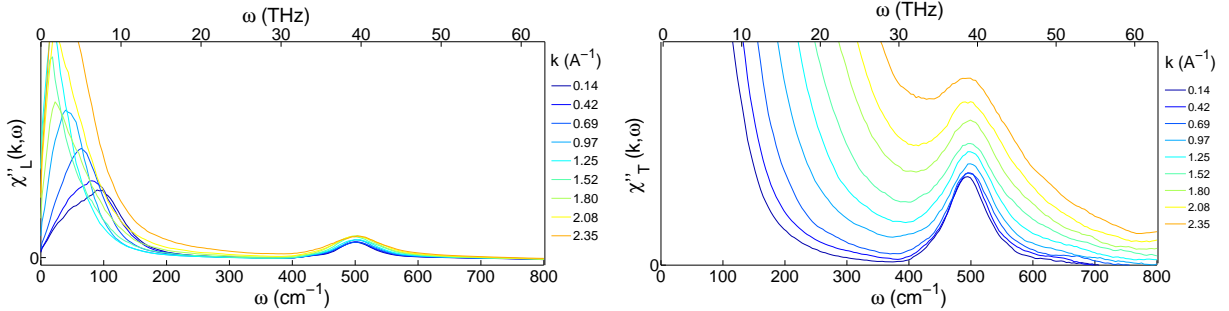


FIG. 5. **Longitudinal (left) and transverse (right) dielectric susceptibility for a system of 1,000 acetonitrile molecules.** The broad band which peaks at 100 cm^{-1} exhibits dispersion. We hypothesize this dispersion is due entirely to the translational modes, however we cannot say for sure since the librational and translational modes overlap in this region. The peak at $\approx 500 \text{ cm}^{-1}$ is due to CCN bending. The static dielectric function $\epsilon(k, 0)$ has not converged properly, so the magnitude of the transverse peaks is not converged correctly, but the position of the peaks and dispersion can be seen.

A. Supplementary info: Examples of fitting

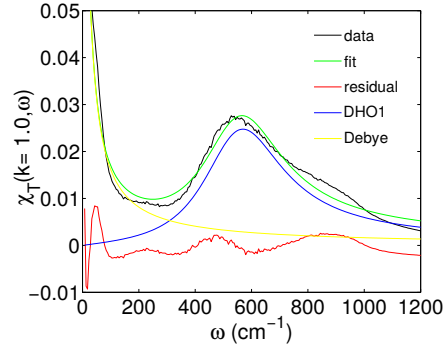


FIG. 6. Example fits of the transverse susceptibility of TIP4P/2005f at 300 K. Fit with a Debye function and one damped harmonic oscillator at $k = .25\text{\AA}^{-1}$ and $k = 1.4\text{\AA}^{-1}$. The residual show the parts not captured by the fit.

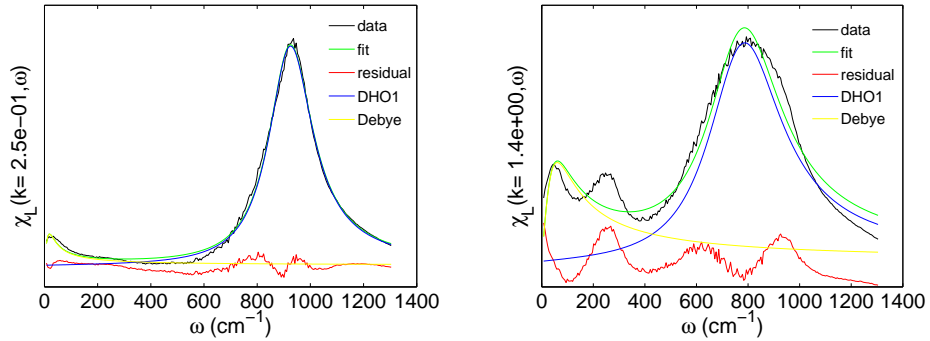


FIG. 7. Example fits of the longitudinal susceptibility of TIP4P/2005f at 300K. Fit with a Debye function and one damped harmonic oscillator at $k = .25\text{\AA}^{-1}$ (left) and $k = 1.4\text{\AA}^{-1}$ (right). Two peaks appear in the residual - the lower frequency peak is dispersive, having the same dispersion relation as the fitted peak, suggesting that it is actually part of the dispersive peak lineshape that is not captured by our lineshape function. The higher frequency peak in the residual is non-dispersive and is in the same location for both the transverse and longitudinal susceptibility.

B. Supplementary info: spatial decomposition of spectra

There are several different ways to decompose a spectra into contributions from molecules separated by distance R :

Kirkwood dipole-sphere method

This is the method we choose, which is a modification of the sphere-sphere method (see below). We start with the time-correlation function of interest :

$$\phi(t) = \left\langle \sum_i \boldsymbol{\mu}_i(0) \cdot \sum_j \boldsymbol{\mu}_j(t) \right\rangle \quad (16)$$

Here $\boldsymbol{\mu}$ can be replaced with any dynamical variable of interest, for instance $\mathbf{p}^T(\mathbf{k}, t)$ or $\mathbf{j}(t)$. We omit the k dependence for simplicity.

The most straightforward way is to limit the molecules around each molecule i to those in a sphere of radius R :

$$\phi(t, R) = \left\langle \sum_i \boldsymbol{\mu}_i(0) \cdot \sum_{j \in R_i} \boldsymbol{\mu}_j(t) \right\rangle \quad (17)$$

This is similar to the method employed by Bopp & Kornyshev. During the the course of a simulation molecules enter and leave each sphere, which creates noise, requiring longer averaging times. This can be improved by utilizing a smooth cutoff function:

$$\phi(t, R) = \left\langle \sum_i \boldsymbol{\mu}_i(0) \cdot \sum_j P_{ij}(t) \boldsymbol{\mu}_j(t) \right\rangle \quad (18)$$

where

$$P_{ij} = \frac{1}{1 + e^{(R_{ij} - R)/D}} \quad (19)$$

Here D is a sharpness parameter determining the relative sharpness of the cutoff. We choose not to use smoothing however, finding it to be unnecessary. The result is a spectra $\chi(\mathbf{k}, \omega, R)$ showing contributions from molecules up to radius R . The resulting function exhibits the expected $R \rightarrow 0$ limit, yielding only the self contribution. In the $R \rightarrow \infty$ limit, the original full response function is recovered. This function can then be numerically differentiated to show the contributions from shells of thickness ΔR centered at distance R .

Sphere-sphere method

Another method discussed by Heyden, et. al. (2010) is to study the *autocorrelation* of the total dipole moment of a sphere of radius R centered around a reference molecule, and then average over each molecule in the system.⁷⁴

$$\phi^P(t, R) = \sum_i \langle \boldsymbol{\mu}_i^P(0) \cdot \boldsymbol{\mu}_i^P(t) \rangle \quad (20)$$

where

$$\boldsymbol{\mu}_i^P(t) = \mathcal{N}_i(t) \sum_{j \in R_i} P_{ij}(t) \boldsymbol{\mu}_j(t) \quad (21)$$

Heyden, et. al. recommend the normalization factor $\mathcal{N}_i(t) = (1 + \sum_{j \in R_i} P_{ij}^2)^{-1/2}$ to normalize for number of molecules in each sphere. This normalization factor is chosen so that in the bulk limit ($R \rightarrow \infty$) the original full response function is obtained (in that limit $\mathcal{N}_i = 1/\sqrt{N_{\text{mol}}}$). In the limit $R \rightarrow 0$ only the self-term contributes. Results from this method must be interpreted with a bit of care since the calculation includes all cross-correlations between molecules within the sphere centered around the reference molecule. We found that this method is more sensitive to intermolecular correlations, in particular the H-bond stretching at $\approx 250 \text{ cm}^{-1}$ (not shown). Altogether though we found the results from this method are complementary with our results from the dipole-sphere method.

Spatial grid method

To achieve higher resolution, Heyden, et. al. also introduce a spatial grid method.⁷⁴ The method works by binning the molecular dipoles into grid cells. To reduce noise caused by molecules moving in and out of bins the binning is Gaussian, meaning the dipoles are smeared with a Gaussian function. Unlike the other methods the spatial grid method does not yield the self part as $R \rightarrow 0$ so this limit requires special interpretation.

C. Supplementary info: calculation of polarization vectors

Bopp & Kornyshev show that to get accurate results in k space it is important to use the polarization vectors for each molecule rather than just the dipole moment. To calculate the polarization vector we use the method of Raineri & Friedman.⁶² We utilize the defining relation for the polarization:

$$\nabla \cdot \mathbf{P}(\mathbf{r}, t) = -\rho(\mathbf{r}, t) \quad (22)$$

When transformed into Fourier space this becomes:

$$i\mathbf{k} \cdot \mathbf{P}(\mathbf{r}, t) = -\rho(\mathbf{k}, t) \quad (23)$$

We introduce polarization vectors for each molecule $\mathbf{p}_i(\mathbf{k})$ so that we have

$$\mathbf{P}(\mathbf{k}) = \sum_i \mathbf{p}_i^{N_{\text{mol}}}(\mathbf{k}) e^{-i\mathbf{k} \cdot \mathbf{r}_i} \quad (24)$$

where

$$i\mathbf{k} \cdot \mathbf{p}_i(\mathbf{k}) = - \sum_{\alpha} q_{\alpha} e^{-i\mathbf{k} \cdot \mathbf{r}_{\alpha i}} \quad (25)$$

The molecules are indexed by i and the atoms on each molecule are indexed by α . $\mathbf{r}_{i\alpha} = \mathbf{r}_i(t) - \mathbf{r}_{\alpha}(t)$ is the distance from each atomic site to the center of mass of molecule i . Following Raineri & Friedman, we use the identity

$$e^x = 1 + x \int_0^1 ds e^{xs} \quad (26)$$

and taking into account the charge neutrality of each molecule we obtain

$$\mathbf{p}_i(\mathbf{k}) = - \sum_{\alpha} q_{\alpha} \mathbf{r}_{\alpha i} \int_0^1 ds e^{-i\mathbf{k} \cdot \mathbf{r}_{\alpha i} s} \quad (27)$$

$$\mathbf{p}_i(\mathbf{k}) = \sum_{\alpha} \frac{q_{\alpha} \mathbf{r}_{\alpha i}}{i\mathbf{k} \cdot \mathbf{r}_{\alpha i}} (e^{i\mathbf{k} \cdot \mathbf{r}_{\alpha i}} - 1) \quad (28)$$

The transverse part is then calculated as $\mathbf{P}_T = \hat{\mathbf{k}} \times \mathbf{P}$, while the longitudinal component is $\mathbf{P}_L = \hat{\mathbf{k}} \cdot \mathbf{P}$. The longitudinal component can also be calculated more directly from:

$$\hat{\mathbf{k}} \cdot \mathbf{P} = \frac{i\rho(\mathbf{k}, t)}{k} = P_L \quad (29)$$

This yields the following Kubo formula for the longitudinal part of the response:

$$\chi_L(\mathbf{k}, \omega) = \frac{\beta}{\epsilon_0 k^2} \int_0^{\infty} dt \frac{d}{dt} \langle \rho(\mathbf{k}, t) \rho^*(\mathbf{k}, 0) \rangle e^{i\omega t} \quad (30)$$

For a system composed of point charges, the charge density is :

$$\rho(\mathbf{r}, t) = \frac{1}{V} \sum_i \sum_{\alpha} q_{i\alpha} \delta(\mathbf{r} - \mathbf{r}_i(t) - \mathbf{r}_{i\alpha}(t)) \quad (31)$$

Again, the index i runs over the molecules while α runs over the atomic sites on each molecule. The charge density in k -space becomes:

$$\rho(\mathbf{k}, t) = \frac{1}{V} \sum_i \sum_{\alpha} q_{\alpha} e^{-i\mathbf{k} \cdot (\mathbf{r}_i(t) + \mathbf{r}_{i\alpha}(t))} \quad (32)$$

Note that this can be Taylor expanded as:

$$\begin{aligned} \frac{\rho(\mathbf{k}, t)}{k} &= \frac{1}{k} \sum_i \sum_{\alpha} q_{\alpha} \sum_n \frac{(-i\mathbf{k} \cdot \mathbf{r}_{i\alpha}(t))^n}{n!} \\ &= \mathbf{M}(\mathbf{k}, t) + \mathbf{Q}(\mathbf{k}, t) + \mathbf{O}(\mathbf{k}, t) + \dots \end{aligned} \quad (33)$$

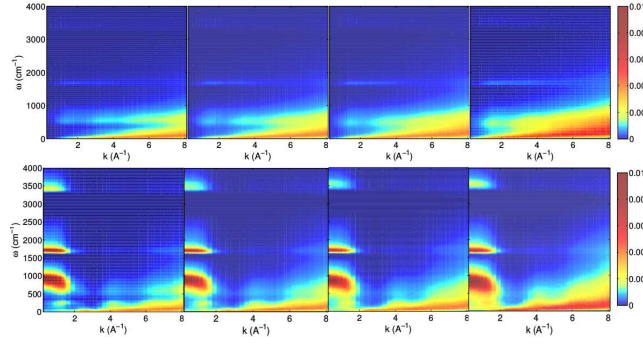


FIG. 8. Imaginary part of the longitudinal (top) and transverse (bottom) polar structure factor for TIP4P/2005f at 250 K, 300 K, 350 K, and 400 K (left to right). Note the increased intensity of the low frequency, high wavenumber intramolecular mode at higher temperatures. This is likely due to weaker H-bonding and greater freedom for inertial motion, which is responsible for this band.

Here $\mathbf{M}(\mathbf{k}, t)$, $\mathbf{Q}(\mathbf{k}, t)$, $\mathbf{O}(\mathbf{k}, t)$ are contributions due to the molecular dipoles, quadrupoles and octupoles. In the limit $k \rightarrow 0$ it from supplementary equation 30 it can be seen that only the dipole term contributes to the susceptibility. In the $k \rightarrow 0$ limit one obtains

$$\chi_L(k, \omega) \approx \frac{\beta}{3\epsilon_0 V} \int_0^\infty dt \frac{d}{dt} \langle \mathbf{M}_L(\mathbf{k}, t) \cdot \mathbf{M}_L^*(\mathbf{k}, 0) \rangle e^{i\omega t} \quad (34)$$

with

$$\mathbf{M}_L(\mathbf{k}, t) = \sum_{i=1}^{N_{\text{mol}}} \hat{\mathbf{k}} \cdot \boldsymbol{\mu}_i(t) e^{i\mathbf{k} \cdot \mathbf{r}_i(t)} \quad (35)$$

This type of expression has been used previously as an approximate expression at small k .⁷⁵ However, Bopp & Kornyshev show quite convincingly that for water the higher order multipole terms are very important, even at the smallest k available in computer simulation.²¹ Neglect of the higher order terms leads to severe consequences at large k , and one will not recover the physical limit $\lim_{k \rightarrow \infty} \chi_{L/T}(k) = 1$ unless higher order terms are included.

D. Supplementary info: polarization-polarization structure factors

To assist in visualizing $\chi_{L,T}(k, \omega)$ we introduce longitudinal and transverse “polarization-polarization structure factors:

$$S_{L,T}^{PP}(k, \omega) = \int_0^\infty \dot{\Phi}_{L,T}(k, t) e^{i\omega t} dt \quad (36)$$

Thus, $\chi_{L,T}(k, \omega) = \chi_{L,T}(k, 0) S_{L,T}^{PP}(k, \omega)$. These plots are shown solely because they provide a nice visual overview of the features in the nonlocal susceptibility. The main novel feature that appears in these plots is the low frequency acoustic-like mode originating at $\approx 60 \text{ cm}^{-1}$. This mode is purely intramolecular in nature and arises from inertial rotation.⁷⁶⁷⁷ At very high wavenumbers ($k > 7$) the relaxation is described by a rapidly decaying exponential and a Gaussian function.⁷⁸

$$\Phi_L(k, t) = A(k) e^{t/\tau_1(k)} + B(k) e^{-(t/\tau_2(k))^2} \quad (37)$$

Gaussian relaxation yields the following equation for the imaginary part of the susceptibility:

$$\begin{aligned} \Phi(k, t) &= B e^{-(t/\tau)^2} \\ \text{Im}\{\chi(k, \omega)\} &= \chi(k, 0) B \frac{\sqrt{\pi}}{2} \omega \tau^2 e^{-\frac{1}{4}\tau^2 \omega^2} \end{aligned} \quad (38)$$

The real part is:

$$\text{Re}\{\chi(k, \omega)\} = \chi(k, 0) B (\tau - \tau^2 \omega F(\omega\tau/2)) \quad (39)$$

where $F()$ is Dawson's integral. The Gaussian form for the correlation function can be derived by considering a free rigid dipole subjected to Brownian kicks. In that case the relaxation function can be computed exactly.⁷⁹

$$\phi(t) = \exp \left[-\frac{t}{\tau_1} + \frac{\tau_2}{\tau_1} \left\{ 1 - \exp \left(-\frac{t}{\tau_2} \right) \right\} \right] \quad (40)$$

where $\tau_1 = \xi/2k_B T$ and $\tau_2 = I/\xi$ and ξ is the friction. In either the limit $\xi \rightarrow 0$ or $t \rightarrow 0$ one obtains the Gaussian form. Thus the interpretation of the Gaussian form is that it is due to fast inertial relaxation. It has been suggested that such inertial relaxation is origin of the Poley absorption that has been found in some dipolar liquids.^{79,80} "Poley absorption" appears to be used as a general term for absorption of unknown origin found in many polar liquids around 10 cm^{-1} (.3 THz),⁸⁰ first described by Poley in 1955.⁸¹ It has been variously described as being due to fast inertial "rattling" of molecules within their potential energy basins or as due to fast librational/inertial motion analogous to the rotational absorption of gas molecules.^{76,77}